AGU PUBLICATIONS

Geophysical Research Letters

RESEARCH LETTER
10.1002/2017GL074911

Key Points:
- Distribution of intraplate volcanism clearly linked to LAB depth variations derived from seismic velocity model
- Evidence for interaction between a passing plume and cavity-induced upwelling beneath non-age-progressive volcanism
- Joint seismic imaging and geodynamic modeling a valuable tool for understanding small-scale convection

Supporting Information:
- Supporting Information S1

Correspondence to:
N. Rawlinson,
nr441@cam.ac.uk

Citation:
Rawlinson, N., D. R. Davies, and S. Pilia (2017), The mechanisms underpinning Cenozoic intraplate volcanism in eastern Australia: Insights from seismic tomography and geodynamic modeling. *Geophys. Res. Lett.*, *44*, 9681–9690, doi:10.1002/2017GL074911.

Received 11 JUL 2017
Accepted 18 AUG 2017
Accepted article online 22 AUG 2017
Published online 13 OCT 2017

©2017. American Geophysical Union. All Rights Reserved.

The mechanisms underpinning Cenozoic intraplate volcanism in eastern Australia: Insights from seismic tomography and geodynamic modeling

N. Rawlinson[1], D. R. Davies[2], and S. Pilia[3]

[1]Department of Earth Sciences-Bullard Labs, University of Cambridge, Cambridge, UK, [2]Research School of Earth Sciences, Australian National University, Canberra, ACT, Australia, [3]Department of Petroleum Geosciences, Petroleum Institute, Abu Dhabi, UAE

Abstract Cenozoic intraplate volcanism is widespread throughout much of eastern Australia and manifests as both age-progressive volcanic tracks and non-age-progressive lava fields. Various mechanisms have been invoked to explain the origin and distribution of the volcanism, but a broad consensus remains elusive. We use results from seismic tomography to demonstrate a clear link between lithospheric thickness and the occurrence, composition, and volume of volcanic outcrop. Furthermore, we find that non-age-progressive lava fields overlie significant cavities in the base of the lithosphere. Based on numerical simulations of mantle flow, we show that these cavities generate vigorous mantle upwellings, which likely promote decompression melting. However, due to the intermittent nature of the lava field volcanics over the last 50 Ma, it is probable that transient mechanisms also operate to induce or enhance melting. In the case of the Newer Volcanics Province, the passage of a nearby plume appears to be a likely candidate. Our results demonstrate why detailed 3-D variations in lithospheric thickness, plate motion, and transient sources of mantle heterogeneity need to be considered when studying the origin of non age-progressive volcanism in continental interiors.

1. Introduction

Evidence of intraplate volcanism can be found throughout the globe, yet it remains a relatively poorly understood phenomenon, with many different mechanisms proposed to explain its provenance [e.g., *Raddick et al.*, 2002; *Conrad et al.*, 2011; *Ballmer et al.*, 2015a]. In Australia, the origin of widespread Cenozoic intraplate volcanism, which traverses almost the entire length of the eastern seaboard (Figure 1), is a subject of considerable uncertainty and debate. One of the key challenges in trying to pinpoint the mechanisms which lead to melting and emplacement is to explain the overlapping presence, in time and space, of both age-progressive and non-age-progressive volcanism [*Wellman*, 1974]. As illustrated in Figure 1, there are two classes of age-progressive volcanism: (i) central volcanoes, which are bimodal shield volcanoes with both basaltic and felsic flows and intrusions; and (ii) the leucitite suite, which are low-volume potassium-rich leucite-bearing lavas. In contrast, the lava field volcanics, which exhibit no evidence of age progression, are almost exclusively basaltic in nature [*Wellman*, 1974]. The age-progressive volcanism, which is also located offshore in the Tasman Sea, has usually been attributed to the presence of one or more mantle plumes [*Wellman*, 1974; *Johnson*, 1989; *Cohen et al.*, 2007; *Sutherland et al.*, 2012; *Jones and Verdel*, 2015; *Davies et al.*, 2015]. In this scenario, a relatively stationary plume generates melt beneath a NNE migrating plate, hence the observed southerly decrease in age of the central volcanoes and leucitites.

A broad consensus on the origins of the lava field volcanics has proven to be more elusive, with proposed models including (i) decompression melting induced by small-scale convection arising from changes in lithospheric thickness [*Demidjuk et al.*, 2007; *Farrington et al.*, 2010; *Davies and Rawlinson*, 2014]; (ii) rift-related processes in the Tasman and Coral seas which involve melt injections from enriched asthenospheric domains into the migrating lithosphere above [*Sutherland et al.*, 2012]; (iii) heat transfer from the Pacific mantle [*Finn et al.*, 2005]; and (iv) transtensional decompression caused by far-field stresses [*Cas et al.*, 2017]. A key consideration in understanding both lava field and age-progressive volcanics is the influence of the lithosphere, which can exert control on the depth (and, hence, pressure) of decompression melting, the occurrence of small-scale

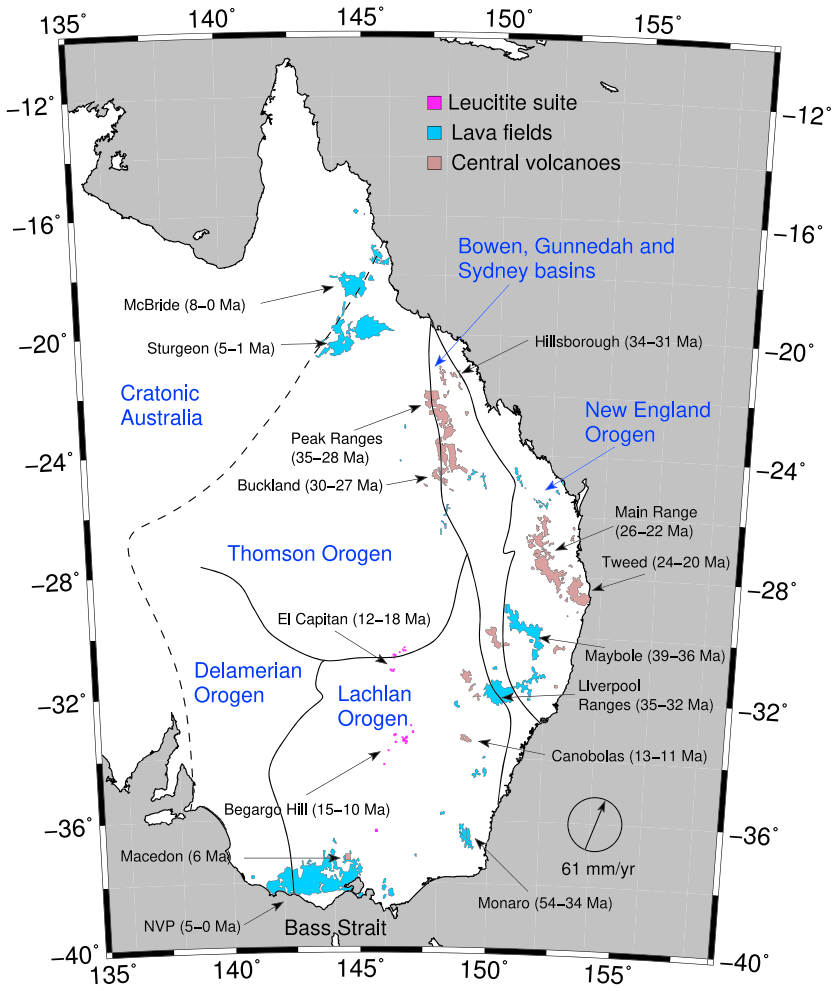

Figure 1. Distribution of eastern Australian Cenozoic intraplate volcanism. Leucitite suite: low-volume potassium-rich leucite-bearing lavas; lava fields: extensive but thin basaltic lava cover sourced from lava cones, small scoria, and maars; and central volcanos: dominantly basaltic and also feature felsic lava flows or intrusions, with lavas emanating from central vents and often producing large volcanic complexes [*Wellman*, 1974]. Ages of rocks associated with age-progressive central volcanos and the leucitite suite are included [e.g., *Johnson*, 1989; *Cohen et al.*, 2009, 2013; *Jones and Verdel*, 2015; *Davies et al.*, 2015]. Direction and rate of current plate motion, based on the model NNR-MORVEL56 [*Argus et al.*, 2011], is shown in the bottom right hand corner of the plot. NVP = Newer Volcanics Province. Black lines indicate the approximate locations of Palaeozoic orogen boundaries [*Glen et al.*, 2016]. Although not shown, recent evidence points to the presence of early to middle Miocene lava fields south of the NVP in Bass Strait [*Reynolds et al.*, 2017].

convection in the upper mantle, the composition of erupted material, and the pathway(s) taken by melt on route to the surface [e.g., *Ashwal and Burke*, 1989; *King and Anderson*, 1998; *Huang et al.*, 2002].

Nearly 20 years ago, the WOMBAT transportable seismic array experiment was conceived with the goal of imaging the lithospheric architecture of eastern Australia at high resolution. To date, 17 sequential deployments have resulted in coverage of the entire Lachlan and Delamerian orogens and parts of the Thomson and New England orogens (see Figure 1 for orogen locations) at a station spacing of approximately 50 km (see Figure S1 in the supporting information). This has allowed high-resolution teleseismic body wave [*Rawlinson et al.*, 2014a, 2015, 2016] and ambient noise surface wave [*Young et al.*, 2013; *Rawlinson et al.*, 2014b; *Pilia et al.*, 2015] tomography to be carried out in order to image the crust and upper mantle. In the results and discussion that follow, we use the latest WOMBAT seismic tomography, combined with numerical modeling of mantle flow, to quantitatively examine the mechanisms underpinning Cenozoic intraplate volcanism in eastern Australia.

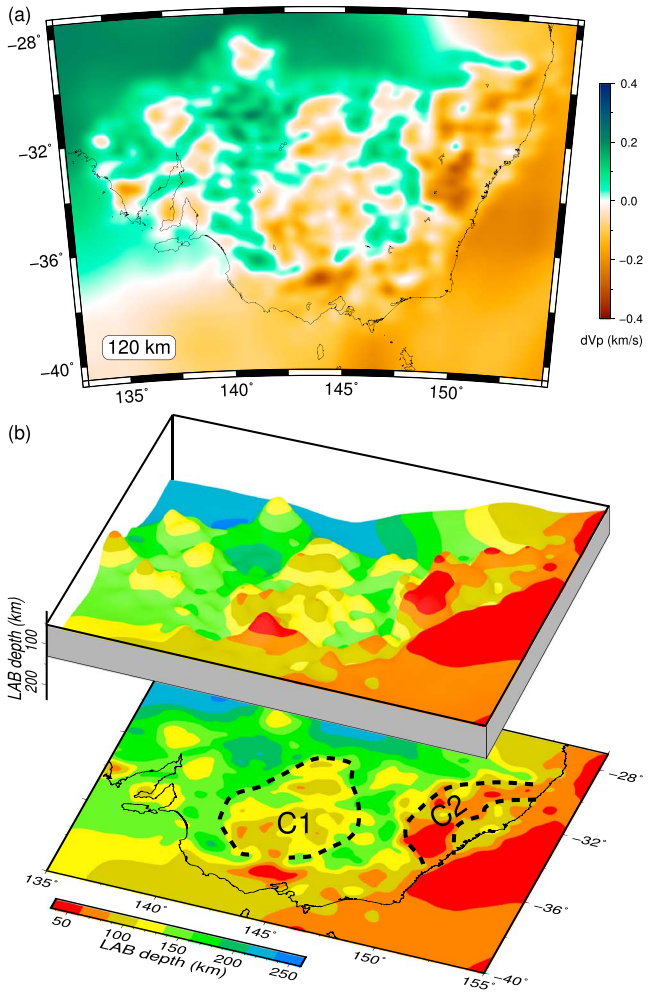

Figure 2. (a) *P* wave velocity perturbations at 120 km depth obtained from teleseismic body wave tomography applied to data recorded by the WOMBAT transportable seismic array. Perturbations are plotted relative to the average velocity at this depth (8.0 km/s). Additional slices and synthetic resolution test results are provided in Figures S2–S4; (b) inferred depth to the base of the lithosphere (LAB), computed from the body wave tomography using the method of *Davies et al.* [2015]. The black dashed line highlights cavities in the base of the lithosphere, which are labeled C1 and C2.

2. Methods and Results

2.1. Teleseismic Body Wave Tomography

FMTOMO [*Rawlinson et al.*, 2006, 2010] is used to invert teleseismic arrival time residuals for perturbations in *P* wave speed in the upper mantle. FMTOMO uses the fast marching method [*Rawlinson and Sambridge*, 2004a, 2004b] to solve the forward problem of travel time prediction, and a subspace inversion method [*Kennett et al.*, 1988] to solve the inverse problem, with nonlinearity addressed by iterative application of the forward and inverse solvers. Crustal structure, which is poorly resolved by the teleseismic data, is accounted for by incorporating a 3-D crustal velocity model derived from ambient noise data (recorded by the WOMBAT array) using a transdimensional tomography scheme [*Young et al.*, 2013]. The regional 3-D AuSREM mantle *P* wave model [*Kennett and Salmon*, 2012] is incorporated in the starting model to account for the use of relative arrival time residuals from different subarrays (see section S1 for more details).

In order to assess the robustness of the solution model, which is shown in Figures 2a and S2, we use synthetic reconstruction tests [*Rawlinson and Spakman*, 2016] that are based on an alternating pattern of discrete spikes which are separated by regions of zero velocity anomaly (see Figure S3). The results show good horizontal resolution (Figure S4) throughout most of the model region, although in the vertical direction, there is a tendency to smear due to the subvertical geometries of the incident rays.

2.2. Depth to Base of Lithosphere (or LAB Depth)

Small-scale convection in the upper mantle has a strong dependence on lithosphere-asthenosphere boundary (LAB) depth variations. In order to completely avoid edge-effects in our 3-D mantle flow calculations (see next section), we use a global model of LAB depth which has three levels of resolution: (i) high, based on the WOMBAT mantle velocity model; (ii) medium, based on AuSREM [*Kennett and Salmon*, 2012]; and (iii) low, based on the GypsumS global model [*Simmons et al.*, 2010]. The main challenge in obtaining a unified multiresolution LAB model is that the WOMBAT model is defined in terms of *P* wave velocity (less sensitive to temperature than *S* wave velocity), is constrained by teleseismic body waves (produces vertical smearing), and is a function of relative arrival time residuals. Consequently, methods that convert seismic velocity to temperature [*Cammarano et al.*, 2003; *Goes et al.*, 2012; *Priestley and McKenzie*, 2013], or use a particular velocity contour or velocity gradient, are unlikely to produce robust results.

Instead, we use a simple empirical method devised by *Davies and Rawlinson* [2014] and *Davies et al.* [2015], which is based on computing the vertically averaged velocity perturbation (dv_{av}) over a prescribed depth range and calibrating it against the minimum and maximum lithosphere thicknesses in the region given by the AuSREM lithosphere thickness model [*Kennett et al.*, 2013]. Using this approach, the minimum dv_{av} will correspond to the thinnest lithosphere, while the maximum dv_{av} will correspond to the thickest lithosphere. Despite the inherent assumptions of this approach, advantages include a decreased sensitivity to vertical smearing and choice of reference model. Figure 2b illustrates the LAB model obtained for southeast Australia using this method. The equivalent Australia-wide model, which is obtained by first embedding the WOMBAT *P* wave model into the AuSREM *P* wave model, is shown in Figure S6a.

For consistency, the same empirical method is applied to the Gypsum *S* wave model, which produces the global LAB model illustrated in Figure S5a. By way of comparison, we also produce LAB models (Figures S5b–S5d) that were calculated by converting the Gypsum *S* wave model to temperature, using lookup tables from the thermodynamic database of *Stixrude and Lithgow-Bertelloni* [2005, 2011], for a simple pyrolitic model of mantle composition, and taking isotherms as a proxy for LAB depth. Since the absolute value of the recovered seismic velocities has a dependence on the choice of reference model and regularization, the absolute value of the isotherm used to define the LAB is not well constrained [e.g., *Goes et al.*, 2005]. For Gypsum, we find that realistic depths are produced by using lower than expected temperatures (1050–1150°C). The best match with the empirical result occurs for a temperature of 1050°C (cf. Figures S5a and S5b), although in general the pattern of depth variations is very similar. The complete multiscale LAB model is obtained by embedding the model of Figure S6a into the model of Figure S5a (see section S2 for more details).

Figure 3a shows a comparison between the new LAB depth model for southeast Australia and the location of Cenozoic volcanic outcrop at the surface, which tends to overlie thin lithosphere. Figure 3b compares the location of a large cavity (C1) in the base of the lithosphere with a total magnetic intensity map, while Figures 3c and 3d (and S7) compare the location of C1 with anisotropic Rayleigh wave phase velocity maps [*Pilia et al.*, 2016] generated using the method of *Debayle and Sambridge* [2004]. These comparisons are discussed in more detail later in the manuscript.

2.3. Numerical Modeling of Mantle Flow

In a recent study *Davies and Rawlinson* [2014] examined mantle flow beneath the NVP using a simple lithospheric thickness model in the presence of plate motion. Both edge-driven convection or EDC (a thermal instability that occurs at the boundary between thick and thin lithosphere) and shear-driven upwelling or SDU (induced by the relative motion between lithosphere and underlying mantle) were considered. Here we apply a similar approach but now directly incorporate the multiscale global LAB model. This represents a major advance on the 2014 study, which computed mantle flow only within a small region surrounding the NVP using a simple block approximation to a previous generation of LAB model. We simulate instantaneous global upper mantle flow using the Fluidity computational modeling framework [e.g., *Davies et al.*, 2011; *Kramer et al.*, 2012; *Le Voci et al.*, 2014; *Davies et al.*, 2016], which employs an unstructured mesh discretization to deal with the multiscale nature of the LAB model. Incompressible mantle flow is simulated under the Boussinesq approximation, and we assume a composite Newtonian and non-Newtonian rheology to accommodate both diffusion and dislocation creep mechanisms. To ensure that the SDU component of mantle flow is accurately captured, present-day plate motions are imposed from the global kinematic model of

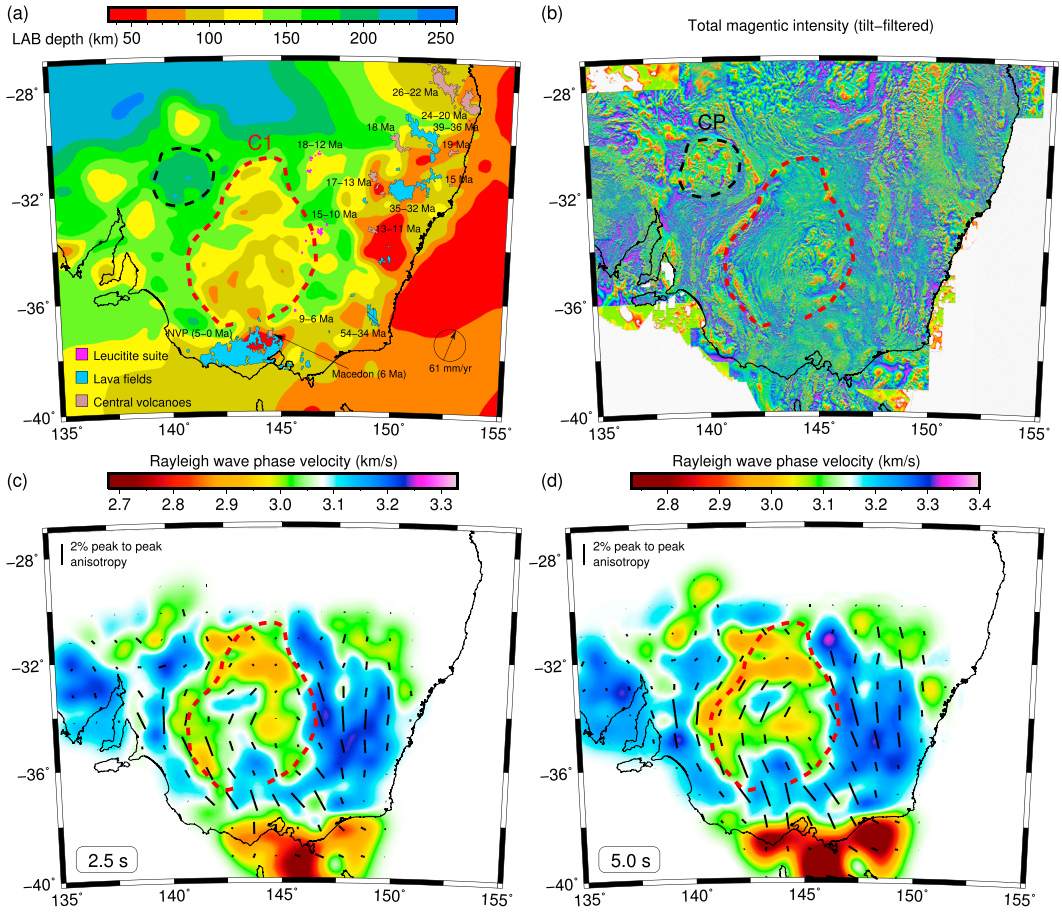

Figure 3. Correlations between crust and lithospheric mantle structure and volcanic outcrop. (a) LAB depth with distribution of Cenozoic volcanism at the surface superimposed (see Figure 1 for description of volcanic outcrop), (b) magnetic map of basement structure, (c) phase velocity map at 2.5 s period (peak sensitivity at ~2.5 km depth), and (d) phase velocity map at 5.0 s period (peak sensitivity at ~5 km depth). See Figure S7 for phase velocity maps at 7.5 s and 12.5 s period. Note that the color scales used in Figures 3c and 3d are not identical. Isotropic velocity variations are displayed as variations in color, while the magnitude and orientation of the fast axis of anisotropy is represented by black lines. Dashed red line delineates the boundary of C1. CP = Curnamona Province.

Seton et al. [2012]. Further details of the method and input parameters, which are constrained by experimental and observational datasets [e.g., *Karato and Wu*, 1993; *Gaboret et al.*, 2003; *Iaffaldano and Lambeck*, 2014] can be found in section S3.

Figure 4a shows one horizontal and two vertical slices through the 3-D radial component of flow (i.e., upwelling and downwelling), which is induced by EDC-SDU (see Figure S8 for radial flow patterns across a range of depths). In order to gain insight into the relative strength of radial and tangential mantle flow beneath southeast Australia, we also plot the velocity ratio (Figure 4b), which is defined as $|Vr/Vt|$, where Vr is the radial velocity and Vt is the velocity magnitude. Thus, $|Vr/Vt|=0$ when there is only tangential flow, and $|Vr/Vt|=1$ when there is only radial flow (see Figure S9 for plots of velocity ratio across a range of depths). The horizontal and vertical slices exhibit clear evidence of upwelling beneath both the large cavity (C1) and smaller cavity (C2) to the east. At shallower depths just beneath the lithosphere, the velocity ratio tends to be smaller due to the increasing dominance of surface plate motions. We note here that the velocity ratio is not intended to be a proxy for where melting may occur; it simply shows the relative dominance of radial and tangential flow. Furthermore, the presence of upwelling does not necessarily imply melting, since this depends on elevating the temperature of material above the solidus at a particular depth. However, the existence of vigorous upwelling at shallower depths (<200 km) beneath the surface expression of lava field volcanism likely provides a favorable setting for decompression melting.

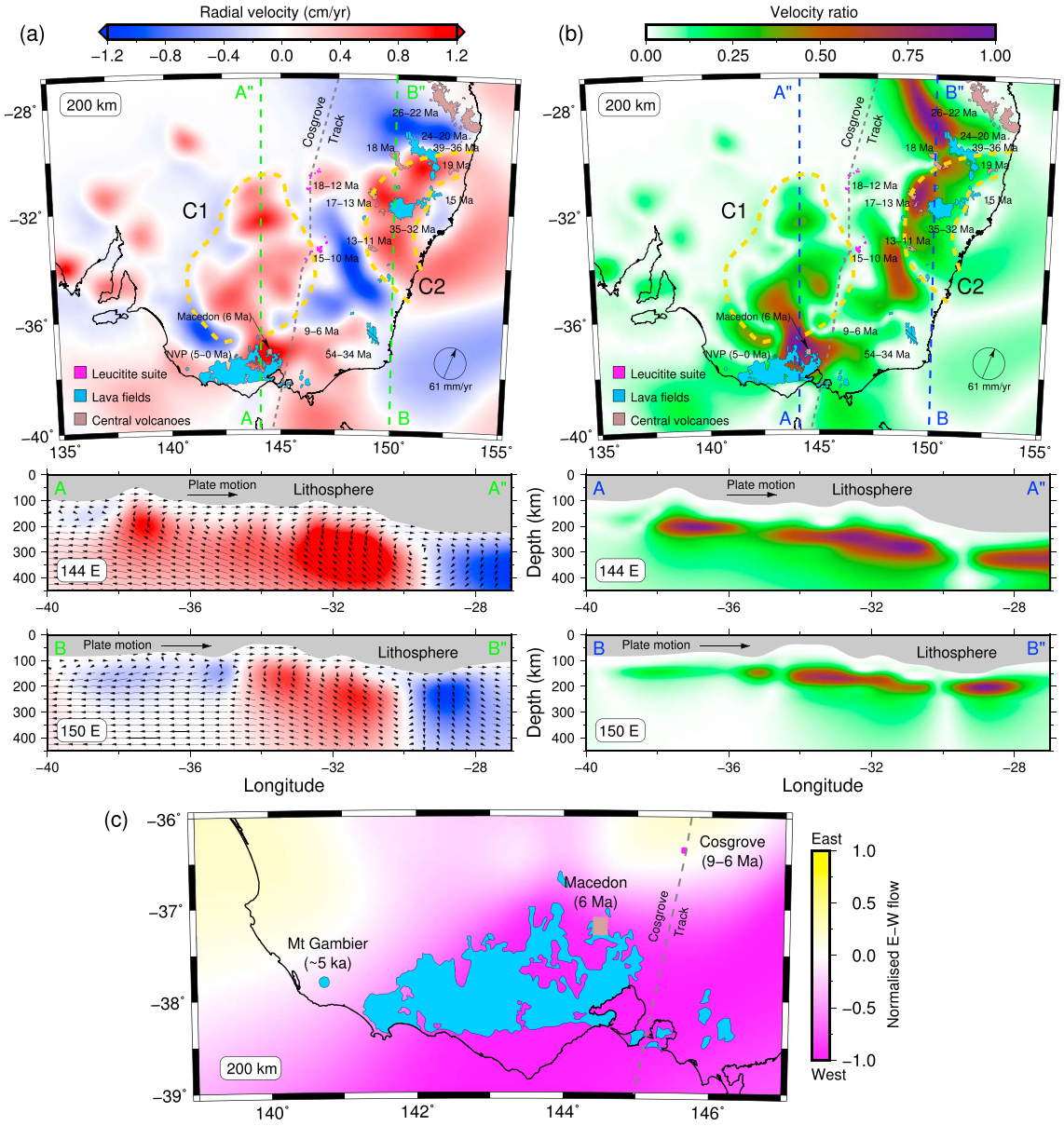

Figure 4. Mantle flow induced by variations in LAB depth and plate motion. (a) Radial mantle flow, with upwellings in red, and downwellings in blue. Small arrows illustrate flow direction in the N-S plane, (b) velocity ratio, with dominantly tangential flow in white/green and dominantly radial flow (upwelling or downwelling) in brown/purple. The boundaries of C1 and C2 are shown by a yellow dashed line. (c) Normalized E-W flow (longitudinal flow divided by magnitude of horizontal flow) in the vicinity of the NVP. Westerly flow is of the order of 2 cm/yr. To determine whether nonzero velocity ratios correspond to upwelling or downwelling, the corresponding plots in Figure 4b can be compared with those in Figure 4a. For plots of radial flow and velocity ratio across a range of depths, refer to Figures S8 and S9.

3. Discussion

The LAB model produced by this study exhibits depth variations in southeast Australia that range from approximately 50 km near the coast to over 200 km in the continental interior (Figure 3a). In some cases, these variations share a close association with near-surface observations. For example, the Curnamona Province (CP), which stands out clearly in total magnetic intensity (Figure 3b), appears as a locally thick region of lithosphere (Figure 3a), which is consistent with its Palaeoproterozoic-Archean origins [*Page*, 2005; *Hand et al.*, 2008]. To the north of the CP, the thicker lithosphere is likely associated with stable shield region of the continent, although it appears to extend further east than previously thought [e.g., *Fishwick et al.*, 2008], possibly due to the presence of a Precambrian continental sliver beneath the southern Thomson Orogen [*Glen et al.*, 2013, 2016]. The New England Orogen, which lies at the very eastern edge of the continent, exhibits zircon

age dates which also suggest the presence of an older continental fragment [*Aitchison et al.*, 1992; *Glen et al.*, 2016], the location of which approximately corresponds with the locally thick zone that forms the eastern margin of C2 (Figure 2b).

A primary feature of the LAB model is the presence of a large cavity in the base of the lithosphere which underlies the Lachlan Orogen (C1 in Figure 2b). This cavity almost exactly underlies a region which exhibits an unusual magnetic fabric (Figure 3b), a prominent low velocity zone in the upper middle crust and a distinct pattern of azimuthal anisotropy (Figures 3c and 3d and S7). The match between the pattern of magnetic fabric and crustal azimuthal anisotropy has been noted previously [*Rawlinson et al.*, 2014a; *Pilia et al.*, 2016] and attributed to the presence of a large orocline beneath the Lachlan Orogen [*Moresi et al.*, 2014]. The western boundary of C1 corresponds to the transition from the Lachlan Orogen to the Delamerian Orogen, which is often regarded as a change from crust of Palaeozoic oceanic origin to crust of Precambrian continental origin [*Glen et al.*, 2013]. The eastern boundary of C1 approximately underlies the transition to the Ordovician Macquarie Arc at the surface [*Foster and Gray*, 2000]. The correlation between C1 (and to a lesser extent C2) and features of the near-surface geology, which are related to Palaeozoic continental accretion, suggests that the cavity predates the onset of Cenozoic intraplate volcanism.

Aside from the correlations noted above, there is also a clear relationship between lithospheric thickness variations, as inferred from seismic body wave tomography, and the occurrence of Cenozoic volcanism in southeast Australia (Figure 3a). The change in volume and composition between the central volcanos (above lithosphere $<$100 km thick) and the leucitite suite (above lithosphere $\sim$130 km thick) can be attributed to suppression of decompression melting beneath thicker lithosphere which, ultimately, produces smaller volumes of lavas containing higher concentrations of incompatible trace elements [*Davies et al.*, 2015].

In order to examine the influence of variations in LAB depth and plate motion on mantle upwelling and hence decompression melting, we carried out 3-D numerical simulations of mantle flow. The most striking result of these tests (Figures 4, S8, and S9) is the effect that C1 and C2, combined with NNE directed plate motion, have on the patterns of mantle flow. In the case of C1, mantle material flows upward into the cavity where it travels south relative to the overriding plate. The narrow southern terminus of C1 combined with increasingly thin lithosphere then focuses flow upward toward the NVP, with peak upwelling rates in excess of 1.2 cm/yr, which is sufficient to cause decompression melting [e.g., *Conrad et al.*, 2010; *Davies and Rawlinson*, 2014]. A similar effect can be observed beneath C2, although in this case intraplate volcanism occurs directly above the cavity; this is probably because the lithosphere is thinner beneath C2 compared to C1 and therefore better able to accommodate decompression melting.

One limitation of the numerical modeling incorporated herein is that it is instantaneous (i.e., flow velocities and viscosities are determined in the presence of a prescribed and fixed temperature/density field): as such, results do not provide insight into the transient nature of lava field volcanism, which range in age from recent to $\sim$40 Ma. Nonetheless, if we assume that the predicted flow regime has not changed markedly in the last 40 Ma (consistent with an invariant plate motion and LAB geometry), then we would have to conclude that small-scale convection, by itself, may be insufficient to produce volcanism at the surface, and some secondary "trigger" is required.

The NVP in southernmost mainland Australia (Figure 3a) is the most recent example of lava field volcanics, with eruptive activity ceasing less than 5 ka [*Wellman*, 1974]. It is one of the best-studied volcanic provinces in Australia, but its origins have remained enigmatic due to a lack of clear evidence for a deep or shallow mantle source. The primary arguments against a plume source includes the east-west distribution of eruptive centers, which is roughly perpendicular to the direction of plate motion, and the lack of an intersecting volcanic chain. However, the newly discovered Cosgrove track [*Davies et al.*, 2015], which includes the leucitite suite shown in Figure 3a, passes just to the east of the NVP at $\sim$6 Ma, roughly 1 million years prior to the first known eruptions. A possible scenario to explain the initialization of volcanism within the NVP is that enriched and elevated temperature plume material becomes entrained in an existing EDC-SDU upwelling (see Figure 4a, which shows how the Cosgrove track intersects the mantle upwelling south of C1); this would locally reduce viscosity, thus enhancing both EDC and SDU [*Ballmer et al.*, 2015b]. Combined with mantle enrichment, this induces or elevates decompression melting to the point where volcanism occurs at the surface. As the plate continues to migrate north, the plume's influence gradually decreases, and volcanism wanes.

The interacting plume scenario finds support in major/trace element and isotopic analyses of basalts from the NVP, which show evidence for intermixing of both plume and shallow mantle derived melt [*McDonough et al.*, 1985]. Furthermore, a similar mechanism has been postulated to explain the Canary volcanic province off the coast of NW Africa [*Geldmacher et al.*, 2005]: here edge drive convection caused by a change in thickness, from the NW African Craton to oceanic lithosphere, is believed to interact with the Canary mantle plume to produce surface volcanism. Our EDC-SDU-plume hypothesis is also consistent with several other recent observations of the NVP [*Oostingh et al.*, 2017], including (i) the largest concentration of volcanic centers occurring close to the eastern margin (nearest to the Cosgrove track), (ii) a decrease in volcanic production rates after 4 Ma (waning influence of passing plume), and (iii) an overall east-west (older-younger) age progression in the volcanism. The latter observation could potentially be explained by dominantly westward mantle flow beneath the NVP, with our model predicting a westward velocity of the order of 2 cm/yr (see Figure 4c).

The lava field volcanism that we associate with C2 is unlikely to originate from the same interaction of EDC-SDU and plume activity that we attribute to the NVP, because the (plume-related) age-progressive volcanism in this region is considerably younger than the lava fields. Therefore, another trigger must be invoked. Possibilities include (i) gradual erosion of overlying lithosphere by the action of long-lived edge-driven convective cells [e.g., *King and Ritsema*, 2000; *Kaislanieimi and van Hunen*, 2014] and (ii) convective entrainment of hydrous lithosphere from the edge of a lithospheric keel or preexisting heterogeneity within the asthenosphere [*Demidjuk et al.*, 2007; *Cas et al.*, 2017], which may locally enhance mantle melting.

4. Conclusions

In this study, we use variations in seismic wave speed derived from teleseismic body wave tomography to infer variations in LAB depth beneath the WOMBAT array in southeast Australia and then perform numerical simulations of 3-D mantle flow to understand how plate motion and LAB depth variations conspire to dictate the pattern of mantle flow beneath the lithosphere. Major findings include (i) a clear correlation between LAB depth and the distribution and composition of Cenozoic intraplate volcanism; (ii) two separate cavity-driven flow regimes that cause mantle upwelling beneath the NVP and an older lava field province on the east coast, with upwelling flow velocities in excess of 1.2 cm/yr; (iii) that EDC-SDU cannot be the sole mechanism underpinning decompression melting and volcanism at the surface due to the temporal nature of lava field provinces; and (iv) that the passage of the Cosgrove track, which intersected the eastern edge of what is now the NVP at ~6 Ma, resulted in enriched and elevated temperature mantle material from the plume becoming entrained within the EDC-SDU upwelling, and instigated a phase of enhanced decompression melting, which gradually migrated westward. These results provide new insight into the dependence of intraplate volcanism on detailed LAB depth variations, plate motion, and transient sources of mantle heterogeneity and therefore have implications for other intraplate volcanic regions around the globe, including in the western US, northeast Asia, Middle East, western Antarctica, and north Africa.

Acknowledgments
We thank Maxim Ballmer and Simon Holford for their constructive comments on the original version of the manuscript. Seismic data, geodynamic models, and seismic velocity models are available, along with format information and links to relevant open-source software, on Figshare using the link https://figshare.com/s/46679f9d7102618e29c7.

References

Aitchison, J. C., T. R. Ireland, M. C. Blake, and P. G. Flood (1992), 530 Ma zircon age for ophiolite from the New England orogen: Oldest rocks known from eastern Australia, *Geology*, *20*, 125–128.

Argus, D. F., R. G. Gordon, and C. DeMets (2011), Geologically current motion of 56 plates relative to the no-net rotation reference frame, *Geochem. Geophys. Geosyst.*, *12*, Q11001, doi:10.1029/2011GC003751.

Ashwal, L. D., and K. Burke (1989), African lithospheric structure, volcanism and topography, *Earth Planet. Sci. Lett.*, *96*, 8–14.

Ballmer, M. D., P. van Keken, G. Ito, and G. Schubert (2015a), Hotspots, large igneous provinces and melting anomalies, *Treatise on Geophys.*, *7*, 371–435.

Ballmer, M. D., C. P. Conrad, E. I. Smith, and R. Johnsen (2015b), Intraplate volcanism at the edges of the colorado plateau sustained by a combination of triggered edge-driven convection and shear-driven upwelling, *Geochem. Geophys. Geosyst.*, *16*, 366–379, doi:10.1002/2014GC005641.

Cammarano, F., S. Goes, P. Vacher, and D. Giardini (2003), Inferring upper-mantle temperatures from seismic velocities, *Phys. Earth Planet. Inter.*, *138*, 197–222.

Cas, R. A. F., J. Van Otterloo, T. N. Blaike, and J. Van Den Hove (2017), The dynamics of a very large intra-plate continental basaltic volcanic province, the Newer Volcanics Province, SE Australia, and implications for other provinces, in *Monogenetic Volcanism, Special Publications*, vol. 446, edited by K. Németh et al., pp. 123–172, Geol. Soc., London.

Cohen, B. E., P. M. Vasconcelos, and K. M. Knesel (2007), $^{40}Ar/^{39}Ar$ constraints on the timing of Oligocene intraplate volcanism in southeast Queensland, *Aust. J. Earth Sci.*, *54*, 105–125.

Cohen, B. E., K. M. Knesel, P. M. Vasconcelos, D. S. Thiede, and J. M. Hergt (2009), $^{40}Ar/^{39}Ar$ constraints on the timing and origin of Miocene leucitite volcanism in southeastern Australia, *Aus. J. Earth Sci.*, *55*, 407–418, doi:10.1090/08120090701769514.

Cohen, B. E., K. M. Knesel, P. M. Vasconcelos, and W. P. Schellart (2013), Tracking the Australian plate motion through the Cenozoic: constraints from $^{40}Ar/^{39}Ar$ geochronology, *Tectonics*, *32*, 1371–1383, doi:10.1002/tect.20084.

Conrad, C. P., B. Wu, E. I. Smith, T. A. Bianco, and A. Tibbetts (2010), Shear-driven upwelling induced by lateral viscosity variations and asthenospheric shear: A mechanism for intraplate volcanism, *Phys. Earth Planet. Inter.*, *178*, 162–175.
Conrad, C. P., T. A. Bianco, E. I. Smith, and P. Wessel (2011), Patterns of intraplate volcanism controlled by asthenospheric shear, *Nat. Geosci.*, *4*, 317–321.
Davies, D. R., and N. Rawlinson (2014), On the origin of recent intra-plate volcanism in Australia, *Geology*, *42*, 1031–1034, doi:10.1130/G36093.1.
Davies, D. R., C. R. Wilson, and S. C. Kramer (2011), Fluidity: A fully unstructured anisotropic adaptive mesh computational modeling framework for geodynamics, *Geochem. Geophys. Geosyst.*, *12*, Q06001, doi:10.1029/2011GC003551.
Davies, D. R., N. Rawlinson, N. Iaffaldano, and I. H. Campbell (2015), Lithospheric controls on magma composition along Earth's longest continental hotspot track, *Nature*, *525*, 511–514.
Davies, D. R., G. Le Voci, S. Goes, S. C. Kramer, and C. R. Wilson (2016), The mantle wedge's transient 3-D flow regime and thermal structure, *Geochem. Geophys. Geosys.*, *17*, 78–100, doi:10.1002/2015GC006125.
Debayle, E., and M. Sambridge (2004), Inversion of massive surface wave data sets: Model construction and resolution assessment, *J. Geophys. Res.*, *109*, B02316, doi:10.1029/2003JB002652.
Demidjuk, Z., S. Turner, M. Sandiford, G. Rhiannon, J. Foden, and M. Etheridge (2007), U-series isotope and geodynamic constraints on mantle melting processes beneath the Newer Volcanic Province in South Australia, *Earth Planet. Sci. Lett.*, *261*, 517–533.
Farrington, R. J., D. R. Stegman, L. N. Moresi, M. Sandiford, and D. A. May (2010), Interactions of 3D mantle flow and continental lithosphere near passive margins, *Tectonophysics*, *483*, 20–28.
Finn, C. A., R. D. Müller, and K. S. Panter (2005), A Cenozoic diffuse alkaline magmatic province (DAMP) in the southwest Pacific without rift or plume origin, *Geochem. Geophys. Geosyst.*, *6*, Q02005, doi:10.1029/2004GC000723.
Fishwick, S., M. Heintz, B. L. N. Kennett, A. M. Reading, and K. Yoshizawa (2008), Steps in lithospheric thickness within eastern Australia, evidence from surface wave tomography, *Tectonics*, *27*, TC4009, doi:10.1029/2007TC002116.
Foster, D. A., and D. R. Gray (2000), Evolution and structure of the Lachlan Fold Belt (Orogen) of eastern Australia, *Ann. Rev. Earth Planet. Sci.*, *28*, 47–80.
Gaboret, C., A. M. Forte, and J. P. Montagner (2003), The unique dynamics of the Pacific Hemisphere mantle and its signature on seismic anisotropy, *Earth Planet. Sci. Lett.*, *208*, 219–233.
Geldmacher, J., K. Hoerne, P. van den Bogaard, S. Duggen, and R. Werner (2005), New $^{40}Ar/^{39}Ar$ age and geochemical data from seamounts in the Canary and Madeira volcanic provinces: Support for the mantle plume hypothesis, *Earth Planet. Sci. Lett.*, *237*, 85–101.
Glen, R. A., R. J. Korsch, R. Hegarty, A. Saeed, Y. P. Djomani, R. D. Costelloe, and E. Belousova (2013), Geodynamic significance of the boundary between the Thomson Orogen and the Lachlan Orogen, northwestern New South Wales and implications for Tasmanide tectonics, *Aust. J. Earth Sci.*, *60*, 371–412.
Glen, R. A., E. Belousova, and W. L. Griffin (2016), Different styles of modern and ancient non-collisional orogens and implications for crustal growth: A Gondwanaland perspective, *Can. J. Earth Sci.*, *53*, 1372–1415.
Goes, S., F. J. Simons, and K. Yoshizawa (2005), Seismic constraints on temperature of the Australian uppermost mantle, *Earth Planet. Sci. Lett.*, *236*, 227–237.
Goes, S., J. Armitage, N. Harmon, H. Smith, and R. Huismans (2012), Low seismic velocities below mid-ocean ridges: Attenuation verses melt retention, *J. Geophys. Res.*, *117*, B12403, doi:10.1029/2012JB009637.
Hand, M., A. Reid, M. Szpunar, N. Direen, B. Wade, J. Payne, and K. Barovich (2008), Crustal architecture during the early Mesoproterozoic Hiltaba-related mineralisation event: Are the Gawler Range Volcanics a foreland basin fill?, *MESA J.*, *51*, 19–24.
Huang, J., D. Zhao, and S. Zheng (2002), Lithospheric structure and its relationship to seismic and volcanic activity in southwest China, *J. Geophys. Res.*, *107*(B10), 2255, doi:10.1029/2000JB000137.
Iaffaldano, G., and K. Lambeck (2014), Pacific plate-motion change at the time of the Hawaiian-Emperor bend constrains the viscosity of Earth's asthenosphere, *Geophys. Res. Lett.*, *15*, 3398–3406, doi:10.1002/2014GL059763.
Johnson, R. W. (1989), *Intraplate Volcanism in Eastern Australia and New Zealand*, Cambridge Univ. Press, New York.
Jones, I., and C. Verdel (2015), Basalt distribution and volume estimates of Cenozoic volcanism in the Bowen Basin region of eastern Australia: Implications for a waning mantle plume, *Aust. J. Earth Sci.*, *62*, 255–263.
Kaislanieimi, L., and J. van Hunen (2014), Dynamics of lithospheric thinning and mantle melting by edge-driven convection: Application to Moroccan Atlas mountains, *Geochem. Geophys. Geosyst.*, *15*, 3175–3189, doi:10.1002/2014GC005414.
Karato, S.-I., and P. Wu (1993), Rheology of the upper mantle: A synthesis, *Science*, *260*, 771–778.
Kennett, B. L. N., and M. Salmon (2012), AuSREM: Australian seismological reference model, *Aust. J. Earth Sci.*, *59*, 1091–1103.
Kennett, B. L. N., M. S. Sambridge, and P. R. Williamson (1988), Subspace methods for large scale inverse problems involving multiple parameter classes, *Geophys. J.*, *94*, 237–247.
Kennett, B. L. N., A. Fichtner, S. Fishwick, and K. Yoshizawa (2013), Australian Seismological Reference Model (AuSREM): Mantle component, *Geophys. J. Int.*, *192*, 871–887, doi:10.1080/08120099.2012.736406.
King, S. D., and D. L. Anderson (1998), Edge-driven convection, *Earth Planet. Sci. Lett.*, *160*, 289–296.
King, S. D., and J. Ritsema (2000), African hotspot volcanism: Small-scale convection in the upper mantle beneath cratons, *Science*, *290*, 1137–1140.
Kramer, S. C., C. R. Wilson, and D. R. Davies (2012), An implicit free-surface algorithm for geodynamical simulations, *Phys. Earth Planet. Int.*, *194*, 25–37, doi:10.1016/j.pepi.2012.01.001.
Le Voci, G., D. R. Davies, S. Goes, S. C. Kramer, and C. R. Wilson (2014), A systematic 2-D investigation into the mantle wedge's transient flow regime and thermal structure: Complexities arising from buoyancy and a hydrated rheology, *Geochem. Geophys. Geosys.*, *15*, 28–51, doi:10.1002/2013GC005022.
McDonough, W. F., M. T. McCulloch, and S. S. Sun (1985), Isotopic and geochemical systematics in Tertiary-Recent basalts from southeastern Australia and implications for the evolution of the sub-continental lithosphere, *Geochim. Cosmochim. Acta*, *49*, 2051–2067.
Moresi, L., P. G. Betts, M. S. Miller, and R. A. Cayley (2014), Dynamics of continental accretion, *Nature*, *508*, 245–248.
Oostingh, K. F., F. Jourdan, E. L. Matchan, and D. Phillips (2017), $^{40}Ar/^{39}Ar$ geochronology reveals rapid change from plume-assisted to stress-dependent volcanism in the Newer Volcanic Province, SE Australia, *Geochem. Geophys. Geosys.*, *18*, 1065–1089, doi:10.1002/2016GC006601.
Page, R. W. (2005), Correlation of Olary and Broken Hill domains, Curnamona Province: Possible relationship to Mount Isa and other north Australian Pb-Zn-Ag-bearing successions, *Econ. Geol.*, *100*, 663–676.
Pilia, S., N. Rawlinson, R. A. Cayley, R. Musgrave, A. M. Reading, N. G. Direen, and M. K. Young (2015), Evidence of micro-continent entrainment during crustal accretion, *Sci. Rep.*, *5*, 8218, doi:10.1038/srep/08,218.

Pilia, S., P. Arroucau, N. Rawlinson, A. M. Reading, and R. A. Cayley (2016), Inherited crustal deformation along the East Gondwana margin revealed by seismic anisotropy tomography, *Geophys. Res. Lett.*, *43*, 12,082–12,090, doi:10.1002/2016GL071201.

Priestley, K., and D. McKenzie (2013), The relationship between shear wave velocity, temperature, attenuation and viscosity in the shallow part of the mantle, *Earth Planet. Sci. Lett.*, *381*, 78–91.

Raddick, M. J., E. M. Parmentier, and D. S. Scheirer (2002), Buoyant decrompression melting: A possible mechanism for intraplate melting, *J. Geophys. Res.*, *107*(B10), 2228, doi:10.1029/2001JB000617.

Rawlinson, N., and M. Sambridge (2004a), Wavefront evolution in strongly heterogeneous layered media using the fast marching method, *Geophys. J. Int.*, *156*, 631–647.

Rawlinson, N., and M. Sambridge (2004b), Multiple reflection and transmission phases in complex layered media using a multistage fast marching method, *Geophysics*, *69*, 1338–1350, doi:10.1190/1.1801950.

Rawlinson, N., and W. Spakman (2016), On the use of sensitivity tests in seismic tomography, *Geophys. J. Int.*, *205*, 1221–1243.

Rawlinson, N., B. L. N. Kennett, and M. Heintz (2006), Insights into the structure of the upper mantle beneath the Murray Basin from 3D teleseismic tomography, *Aust. J. Earth Sci.*, *53*, 595–604.

Rawlinson, N., H. Tkalčić, and A. M. Reading (2010), Structure of the Tasmanian lithosphere from 3-D seismic tomography, *Aust. J. Earth Sci.*, *57*, 381–394.

Rawlinson, N., M. Salmon, and B. L. N. Kennett (2014a), Transportable seismic array tomography in southeast Australia: Illuminating the transition from Proterozoic to Phanerozoic lithosphere, *Lithos*, *189*, 65–76.

Rawlinson, N., P. Arroucau, R. Musgrave, R. Cayley, M. Young, and M. Salmon (2014b), Complex continental growth along the proto-Pacific margin of East Gondwana, *Geology*, *42*, 783–786.

Rawlinson, N., B. L. N. Kennett, M. Salmon, and R. A. Glen (2015), Origin of lateral heterogeneities in the upper mantle beneath south-east Australia from seismic tomography, in *The Earth's Heterogeneous Mantle: A Geophysical, Geodynamical and Geochemical Perspective*, edited by A. Khan and F. Deschamps, pp. 47–78, Springer, Cham.

Rawlinson, N., S. Pilia, M. Young, M. Salmon, and Y. Yang (2016), Crust and upper mantle structure beneath southeast Australia from ambient noise and teleseismic tomography, *Tectonophysics*, *689*, 143–156.

Reynolds, P., N. Schofiled, R. J. Brown, and S. P. Holford (2017), The architecture of submarine monogenetic volcanoes—Insights from 3D seismic data, *Basin Res.*, doi:10.1111/bre.12230.

Seton, M. et al. (2012), Global continental and ocean basin reconstructions since 200 Ma, *Earth Sci. Rev.*, *113*, 212–270, doi:10.1016/j.earscirev.2012.03.002.

Simmons, N. A., A. M. Forte, L. Boschi, and S. P. Grand (2010), GyPSuM: A joint tomographic model of mantle density and seismic wave speeds, *J. Geophys. Res.*, *115*, B12310, doi:10.1029/2010JB007631.

Stixrude, L., and C. Lithgow-Bertelloni (2005), Thermodynamics of mantle minerals—I. Physical properties, *Geophys. J. Int.*, *162*, 610–632, doi:10.1111/j.1365-246X.2005.02642.x.

Stixrude, L., and C. Lithgow-Bertelloni (2011), Thermodynamics of mantle minerals—II. Phase equilibria, *Geophys. J. Int.*, *184*, 1180–1213, doi:10.1111/j.1365-246X.2010.04890.x.

Sutherland, F. L., I. T. Graham, S. Meffre, H. Zwingmann, and R. E. Pogson (2012), Passive-margin prolonged volcanism, East Australian Plate: Outbursts, progressions, plate controls and suggested causes, *Aust. J. Earth Sci.*, *59*, 983–1005.

Wellman, P. (1974), Potassium-argon ages of the Cainozoic volcanic rocks of eastern Australia, *J. Geol. Soc. Aust.*, *21*, 359–376.

Young, M. K., R. A. Cayley, M. A. McLean, N. Rawlinson, P. Arroucau, and M. Salmon (2013), Crustal structure of the east Gondwana margin in southeast Australia revealed by transdimensional ambient seismic noise tomography, *Geophys. Res. Lett.*, *40*, 4266–4271, doi:10.1002/grl.50878.